The rhizobial type III effector ErnA confers the ability to form nodules in legumes

Albin Teulet[a], Nicolas Busset[b], Joël Fardoux[a], Djamel Gully[a], Clémence Chaintreuil[a], Fabienne Cartieaux[a], Alain Jauneau[c], Virginie Comorge[d], Shin Okazaki[e], Takakazu Kaneko[f], Frédéric Gressent[a], Nico Nouwen[a], Jean-François Arrighi[a], Ralf Koebnik[g], Peter Mergaert[b], Laurent Deslandes[d], and Eric Giraud[a,1]

[a]Institut de Recherche pour le Développement, Laboratoire des Symbioses Tropicales et Méditerranéennes, UMR Institut de Recherche pour le Développement/SupAgro/Institut National de la Recherche Agronomique/Université de Montpellier/Centre de Coopération Internationale en Recherche Agronomique pour le Développement, 34398 Montpellier Cedex 5, France; [b]Institute for Integrative Biology of the Cell, UMR 9198, CNRS/Université Paris-Sud/Commissariat à l'Energie Atomique, 91198 Gif-sur-Yvette, France; [c]CNRS, Plateforme Imagerie-Microscopie, Fédération de Recherche FR3450, 31326 Castanet-Tolosan, France; [d]LIPM, Université de Toulouse, INRA, CNRS, 31326 Castanet-Tolosan, France; [e]Department of International Environmental and Agricultural Science, Graduate School of Agriculture, Tokyo University of Agriculture and Technology, Tokyo 183-8509, Japan; [f]Faculty of Life Sciences, Kyoto Sangyo University, Motoyama, Kamigamo, Kyoto 603-8555, Japan; and [g]Institut de Recherche pour le Développement, Centre de Coopération Internationale en Recherche Agronomique pour le Développement, Université de Montpellier, Interactions Plantes–Microorganismes–Environnement, 34394 Montpellier, France

Edited by Graham C. Walker, Massachusetts Institute of Technology, Cambridge, MA, and approved August 28, 2019 (received for review March 14, 2019)

Several *Bradyrhizobium* species nodulate the leguminous plant *Aeschynomene indica* in a type III secretion system-dependent manner, independently of Nod factors. To date, the underlying molecular determinants involved in this symbiotic process remain unknown. To identify the rhizobial effectors involved in nodulation, we mutated 23 out of the 27 effector genes predicted in *Bradyrhizobium* strain ORS3257. The mutation of *nopAO* increased nodulation and nitrogenase activity, whereas mutation of 5 other effector genes led to various symbiotic defects. The *nopM1* and *nopP1* mutants induced a reduced number of nodules, some of which displayed large necrotic zones. The *nopT* and *nopAB* mutants induced uninfected nodules, and a mutant in a yet-undescribed effector gene lost the capacity for nodule formation. This effector gene, widely conserved among bradyrhizobia, was named *ernA* for "effector required for nodulation-A." Remarkably, expressing *ernA* in a strain unable to nodulate *A. indica* conferred nodulation ability. Upon its delivery by *Pseudomonas fluorescens* into plant cells, ErnA was specifically targeted to the nucleus, and a fluorescence resonance energy transfer–fluorescence lifetime imaging microscopy approach supports the possibility that ErnA binds nucleic acids in the plant nuclei. Ectopic expression of *ernA* in *A. indica* roots activated organogenesis of root- and nodule-like structures. Collectively, this study unravels the symbiotic functions of rhizobial type III effectors playing distinct and complementary roles in suppression of host immune functions, infection, and nodule organogenesis, and suggests that ErnA triggers organ development in plants by a mechanism that remains to be elucidated.

Bradyrhizobium | T3SS | symbiosis | nodulation | legume

Bradyrhizobia are Gram-negative soil bacteria that are widely used in agriculture. They are applied as biofertilizers to sustain the production of crops of agronomic importance (e.g., soybean, peanut, cowpea), thus circumventing the need to add chemical nitrogen fertilizers. Their agronomic interest results from their ability to interact symbiotically with some leguminous plants. This interaction leads to the formation of a new organ, the nodule, in which the bacteria fix nitrogen for the plant's benefit and where, in exchange, the plant provides a protective niche and carbon sources.

The symbiotic process is initiated when the plant perceives specific lipochitooligosaccharide signal molecules, called Nod factors (NFs), which are synthetized and secreted after activation of bacterial nodulation (*nod*) genes by specific plant flavonoids (1). The perception of NFs activates a genetic program leading to 2 coordinated processes, the formation of a nodule and its intracellular infection by the bacteria (2). Beyond these first stages initiated by NF perception, the development of a functional nodule and maintenance of a chronic infection of the nodule cells by bacteria largely relies on the ability of the bacteria to suppress the plant immune system (3). Different strategies have evolved in rhizobia to escape plant immunity (4, 5), but one of the most remarkable is the type III secretion system (T3SS), which is a common and well-described weapon used by bacterial plant pathogens (6).

The T3SS apparatus is a nanosyringe or "injectisome" that traverses the bacterial and eukaryotic cell envelope for direct delivery of type III effector (T3E) proteins into the eukaryotic host cell (7). Like pathogenic bacteria, some rhizobia possess a T3SS encoded by the *rhc* (rhizobium conserved) gene cluster, and secrete T3Es, also named "Nop" (for nodulation outer protein), during the nodulation process (8). These effectors are Janus-faced depending on the host plant (9, 10). On the one hand, they promote symbiosis by suppressing specific plant defense responses, while on the other hand, they trigger activation of plant immune responses called ETI (effector-triggered immunity) upon specific recognition by plant immune receptors (resistance [R] proteins). ETI is often associated with a hypersensitive cell

Significance

Legumes have a tremendous ecological and agronomic importance due to their ability to interact symbiotically with nitrogen-fixing rhizobia. In most of the rhizobial–legume symbioses, the establishment of the interaction requires the plant perception of the bacterial lipochitooligosaccharide Nod factor signal. However, some bradyrhizobia can activate the symbiosis differently, thanks to their type III secretion system, which delivers effector proteins into the host cell. Here, we demonstrate that this symbiotic process relies on a small set of effectors playing distinct and complementary roles. Most remarkably, a nuclear-targeted effector named ErnA conferred the ability to form nodules. The understanding of this alternative pathway toward nitrogen-fixing symbiosis could pave the way for designing new strategies to transfer nodulation into cereals.

Author contributions: A.T., R.K., P.M., L.D., and E.G. designed research; A.T., N.B., J.F., D.G., C.C., F.C., A.J., V.C., S.O., T.K., F.G., N.N., J.-F.A., and E.G. performed research; A.T., N.B., J.F., D.G., C.C., F.C., A.J., V.C., S.O., T.K., F.G., N.N., J.-F.A., P.M., L.D., and E.G. analyzed data; and A.T., P.M., L.D., and E.G. wrote the paper.

The authors declare no conflict of interest.

This article is a PNAS Direct Submission.

[1]To whom correspondence may be addressed. Email: eric.giraud@ird.fr.

This article contains supporting information online at www.pnas.org/lookup/suppl/doi:10.1073/pnas.1904456116/-/DCSupplemental.

First published October 7, 2019.

death response, which halts the infection and renders the interaction incompatible (11, 12).

It was recently shown that the role of the T3SS in the symbiosis was not restricted to the modulation of plant immunity. Indeed, the nodulation of the *Glycine max* cv. Enrei and its *nfr* mutant affected in NF perception can be induced in a T3SS-dependent manner by a *Bradyrhizobium elkanii* USDA61 mutant strain unable to produce NFs (13). This shows that, besides interfering with the plant immune system, some Nop effectors also trigger nodulation by bypassing the NF signal. This T3SS-dependent symbiosis is widespread among bradyrhizobia since a diverse range of nonphotosynthetic *Bradyrhizobium* strains are able to elicit nodules on some *Aeschynomene* species, including *A. indica*, in the absence of NFs (14). Interestingly, depending on the *Bradyrhizobium* strain concerned, a gradient in the outcome of the symbiotic interaction has been observed. The plant response ranged from the induction of nodules which are only infected intercellularly (e.g., *B. elkanii* USDA61) to the induction of nodules in which the host cells are intracellularly invaded and display weak nitrogenase activity (e.g., *Bradyrhizobium* sp. ORS3257, previously named STM6978) (14). This new type of symbiosis is an NF-independent and T3SS-dependent process, as opposed to the one used by some photosynthetic *Bradyrhizobium* strains (ORS278 and BTAi1) that are able to induce functional nodules on some *Aeschynomene* species despite the absence of *nod* and *T3SS* genes (15).

The aim of this study was to better understand the molecular bases of this alternative NF-independent, T3SS-dependent symbiotic process. To identify the effectors controlling the symbiosis, we mutated most of the predicted *nop* effector genes in the genome of strain ORS3257 and analyzed the symbiotic properties of the mutant strains on *A. indica*. We found that this nodulation relies on a restricted set of T3Es playing distinct roles. Remarkably, among the T3Es, we identified the nuclear targeted ErnA effector, which confers the ability to nodulate *A. indica*.

Results

Prediction of the T3E Repertoire in ORS3257. In rhizobia, expression of both *T3SS* and *T3E* genes is controlled by the regulator TtsI, which binds to a highly conserved DNA sequence (the *tts* box) found in the promoter region of target genes to activate their transcription (16, 17). To predict the T3E repertoire of strain ORS3257, we combined 2 *in silico* searches: 1) a TBlastN search of the genome for effectors previously identified in other rhizobia, and 2) a HMMER search for the *tts* box motif using a hidden Markov model (*SI Appendix*, Table S1 and Fig. S1). This analysis retrieved 27 putative effector genes (*SI Appendix*, Table S2), all of which were located in the symbiotic island and distributed in 2 distinct regions, one containing genes encoding the T3SS machinery and the other one containing the *nod* genes (Fig. 1). Among these 27 candidate effector genes, some are commonly found in rhizobia (*nopP*, *nopT*, *nopM*, *nopL*, and *nopC*), some are specifically found in *Bradyrhizobium* strains (*nopAB*, *nopAC*, *nopAD*, *nopAL*, *nopAJ*, *nopAO*, *nopAR*, and *nopBW*), and 9 encode putative new effectors (*SI Appendix*, Table S2).

Several T3Es Are Required for the Establishment of a Functional NF-Independent, T3SS-Dependent Symbiosis on *A. indica*. To identify T3Es involved in the establishment of the symbiosis between strain ORS3257 and *A. indica*, we mutated most of the candidate genes. To optimize the number of mutants to generate, 1 of 2 strategies was used depending on the genetic organization of the candidate genes: 1) "isolated" genes were inactivated by inserting the nonreplicative plasmid pVO155, or 2) genomic regions with several clustered effector genes were deleted using double crossing-over. Altogether, 10 mutants (5 insertion and 5 deletion mutants) covering 23 out of the 27 putative effectors were constructed (Fig. 1*A*). Four candidate genes were excluded from this mutagenesis (*nopAM*, which is located directly upstream of *ttsI* and *rhcC2*, and *nopC*, *nopAL*, and *Brad3257_7768*, which belong to an operon that encodes several T3SS components) (Fig. 1*A*). These genes were not considered during this mutagenesis because it is not yet clear if they encode bona fide effectors or accessory components of the T3SS machinery and because their mutation could have polar effects leading to misinterpretation of nodulation phenotypes.

As previously observed (14), mutation of the secretion machinery (in the Δ*T3SS* mutant) prevented nodulation (Fig. 1 *B* and *C*). Out of the 10 mutants affected in putative effector genes, 6 behaved like the wild-type (WT) strain in terms of the number of nodules, nitrogenase activity, and nodule features (Fig. 1*B*). Interestingly, the symbiotic properties of the 4 remaining mutants (Δ*regA*, Δ*regB*, Δ*regD*, and Ω*7701*) were altered (Fig. 1 *B* and *C*).

The Δ*regA* mutant was significantly impacted in its ability to induce nodules (Fig. 1*B* and *SI Appendix*, Fig. S2). Furthermore, the nodules showed large necrotic zones and very weak nitrogenase activity (Fig. 1 *B* and *C*). Live–dead staining of nodule sections revealed that many of the intracellularly infecting bacteria were dead, as shown by the red propidium iodide staining (Fig. 1*D*). These observations suggest that the region deleted in the Δ*regA* mutant plays an important role in the suppression of plant immunity. Region A encodes 2 putative effectors, NopM1 and NopP1, which, in other rhizobia, have been suggested to interfere with the activation of plant defense responses (18, 19). To identify which one plays a symbiotic role, individual insertional mutants were generated. As shown in *SI Appendix*, Fig. S2, both Ω*nopM1* and Ω*nopP1* mutants displayed a symbiotic phenotype intermediate between the WT strain and the Δ*regA* mutant. This finding suggests that the phenotype of the Δ*regA* mutant results from the cumulative effect of the lack of these 2 effectors, each of which makes an incremental contribution to immune suppression.

The second mutant, Δ*regB*, led to the formation of slightly more nodules than the WT strain but the nodules did not fix nitrogen (Fig. 1*B*). Furthermore, most of the nodules had no central infected tissue and only intercellular bacteria were observed (Fig. 1 *C* and *D* and *SI Appendix*, Fig. S3*E*). Region B contains 2 putative effector genes, *nopT* and *nopAO*, 1 of which is preceded by a *tts* box (*nopT*), and 2 additional *tts* boxes without a clearly defined downstream coding sequence (Fig. 1 and *SI Appendix*, Fig. S3). To better understand the phenotype of the Δ*regB* mutant, 4 additional mutants were studied. Two insertion mutations were generated in *nopT* and *nopAO* (Ω*nopT* and Ω*nopAO*) and 2 deletion mutations (Δ*regB-1* and Δ*regB-2*) were constructed, encompassing the region surrounding the 2 *tts* boxes (*SI Appendix*, Fig. S3). Two of these mutants displayed distinct phenotypes. The plants inoculated with the Ω*nopAO* mutant had more nodules and increased nitrogenase activity (*SI Appendix*, Fig. S3*B*), suggesting that NopAO can have a negative effect on symbiotic efficiency. On the other hand, the Ω*nopT* mutant led to a phenotype similar to that of the Δ*regB* mutant, since no nitrogenase activity was detected and most of the formed nodules were not infected (*SI Appendix*, Fig. S3 *B* and *D*). This observation shows that the phenotype of Δ*regB* was mainly due to the absence of *nopT*, which is required for efficient nodule infection.

The phenotype of the third mutant, Δ*regD*, was very similar to that of Δ*regB* (Fig. 1 *B–D*). This region contains 2 predicted effector genes, *nopAB* and *Brad3257_7707*. Individual mutation of *nopAB* (Ω*nopAB*) led to the same phenotype as observed for the Δ*regD* mutant, whereas the other mutation (Ω*7707*) had no particular symbiotic defect (*SI Appendix*, Fig. S4). These findings show that, like NopT, NopAB is required for efficient nodule infection.

Finally, the most drastic phenotype was observed with the Ω*7701* insertional mutant in which the predicted effector gene *Brad3257_7701* was disrupted. This mutant displayed an apparent Nod⁻ phenotype (absence of nodule formation); microscopic examination revealed only the formation of rare uninfected bump-like

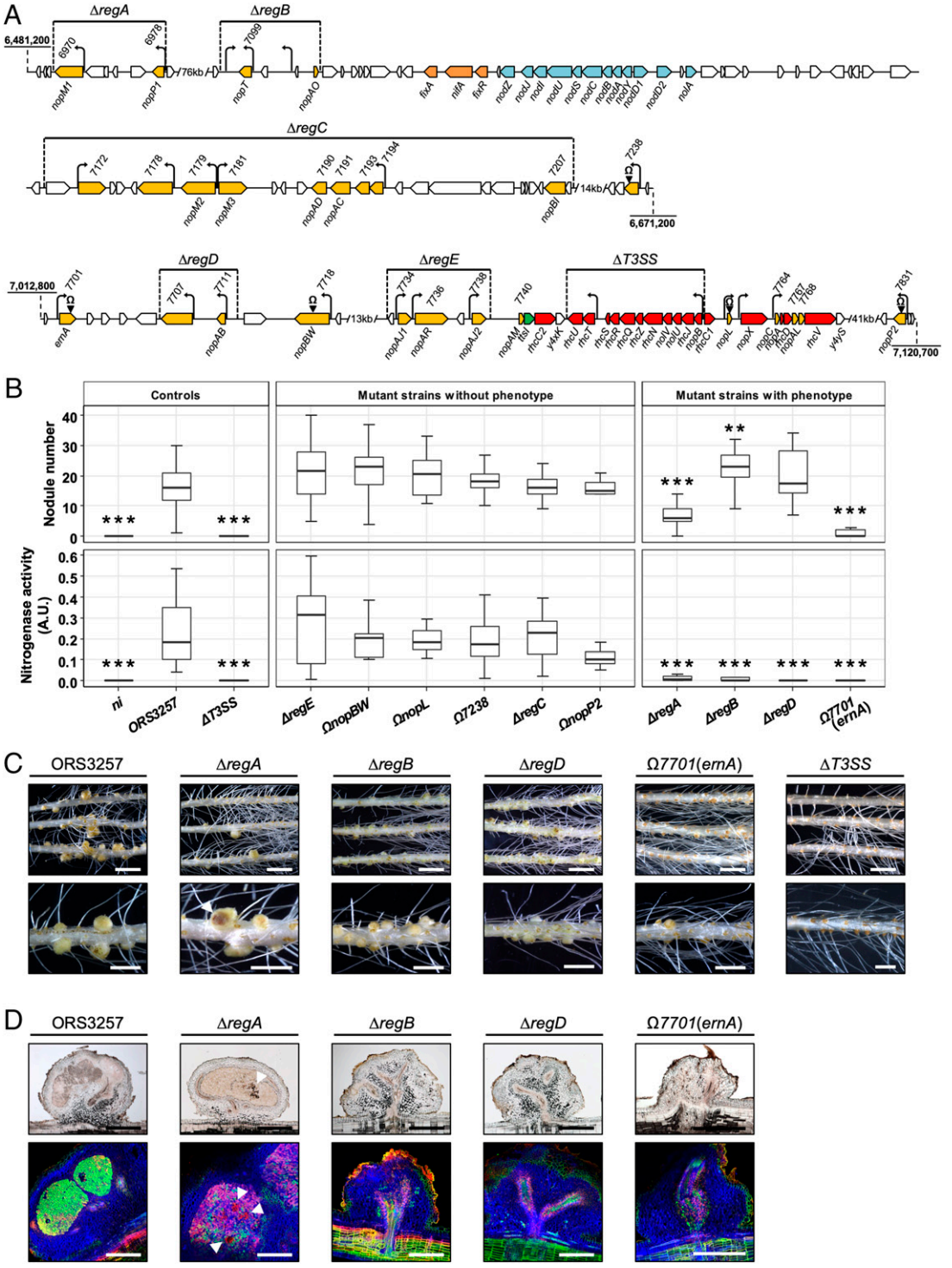

Fig. 1. Identification of T3Es in *Bradyrhizobium* strain ORS3257 that play a symbiotic role in the interaction with *Aeschynomene indica*. (*A*) Genetic organization of putative effector genes identified in strain ORS3257. Deleted regions in the mutants are indicated by horizontal lines. Insertion mutants are indicated by black arrowheads carrying the Ω sign. In yellow, putative effector genes; in orange, *nif* and *fix* genes; in blue, *nod* genes; in red, genes encoding components of the T3SS apparatus; in green, the *ttsI* gene encoding the T3SS transcriptional regulator; black arrows, *tts* boxes. (*B*) Number of nodules formed and nitrogen fixation activity of *A. indica* plants at 21 d after inoculation with strain ORS3257 and its mutant derivatives. Nitrogen fixation activity was measured by the acetylene reduction assay; A.U., arbitrary unit. Box plots show results of 1 representative experiment out of at least 2 independent experiments per strain (18 plants each). The central rectangle spans the first quartile to the third quartile; the bold segment inside the rectangle shows the median; and the whiskers above and below the box show the locations of the maximum and minimum value, respectively. $^{**}P < 0.01$, and $^{***}P < 0.001$, significant differences between WT ORS3257 and each mutant strain using a nonparametric Kruskal–Wallis test. (*C*) View of the root and the nodules induced by strain ORS3257 and its mutant derivatives. (Scale bars: *Upper*, 1.5 cm; *Lower*, 4 mm.) (*D*) Cytological analysis of the nodules induced by strain ORS3257 and its mutant derivatives observed by light (*Upper*) and confocal microscopy (*Lower*) after staining with SYTO 9 (green; live bacteria), calcofluor (blue; plant cell wall), and propidium iodide (red; infected plant nuclei and dead bacteria or bacteria with compromised membranes). (Scale bars, 500 μm.) In *C* and *D*, the white arrowheads indicate necrotic zones.

structures on a few plants (Fig. 1 *B–D* and *SI Appendix*, Fig. S5 *A* and *B*). To confirm that the phenotype of the Ω*7701* mutant was due to the inactivation of *Brad3257_7701* and not because of a polar effect, a complete deletion mutant was constructed (Δ*7701*) into which the WT gene was subsequently reintroduced (Δ*7701*::*7701*). As shown in *SI Appendix*, Fig. S5, the phenotype of Δ*7701* was similar to that of Ω*7701*, whereas Δ*7701*::*7701* displayed a WT phenotype, confirming that the *Brad3257_7701* effector gene is necessary for nodule formation.

This mutagenesis analysis indicates that at least 5 effectors (NopP1, NopM1, NopAB, NopT, and Brad3257_7701) are required for the establishment of the NF-independent, T3SS-dependent symbiosis. Given its importance for nodulation, we next focused on the functional characterization of the Brad3257_7701 effector, hereafter referred to as "ErnA" for "effector required for nodulation-A."

ErnA Is a Bona Fide Type III Effector. The *ernA* gene was predicted to encode a T3E because of the presence of a *tts* box in its upstream coding region. To investigate the regulation of *ernA* in more detail, its expression was monitored in the absence and presence of genistein, a flavonoid known to induce *nod* and *T3SS* genes in *Bradyrhizobium* strains (16). qRT-PCR analysis showed that expression of *ernA* was 3-fold higher in the presence of genistein and that this up-regulation required the presence of the TtsI regulator (Fig. 2*A*), similarly to what was observed for the 2 *T3SS* genes (*rhcJ* and *nopX*) that had been included as controls in this experiment.

Homologs of *ernA* are found in several *Bradyrhizobium* strains (see below), but to our knowledge a possible role as a T3E has not been reported to date. To demonstrate that ErnA is secreted via the T3SS machinery, a His_6-tagged version of ErnA (ErnA-His_6) was expressed in ORS3257, thanks to the introduction of a pVO155-npt2-GFP plasmid carrying the tagged gene, which also constitutively expressed a cytosolic green fluorescent protein (GFP), used here as a control to detect cell lysis. For the purpose of comparison, a His_6-tagged version of the well-known NopT effector was also generated (20, 21). Immunoblot analysis of ErnA-His_6 and NopT-His_6 with an anti-His_6 antibody (α-His) led to the detection of ErnA and NopT in both the culture supernatant and in the cell pellet, while cytosolic GFP, detected with an anti-GFP antibody (α-GFP), was only observed in the cell pellet, confirming the absence of cytosolic proteins in the culture supernatant due to cell lysis (Fig. 2*B*). When expressed in a Δ*T3SS* mutant of ORS3257, ErnA-His_6 and NopT-His_6 were only detected in the cell pellet (Fig. 2*C*). Together, these data confirm that, like the previously characterized NopT protein (20, 21), ErnA is a type III-secreted protein.

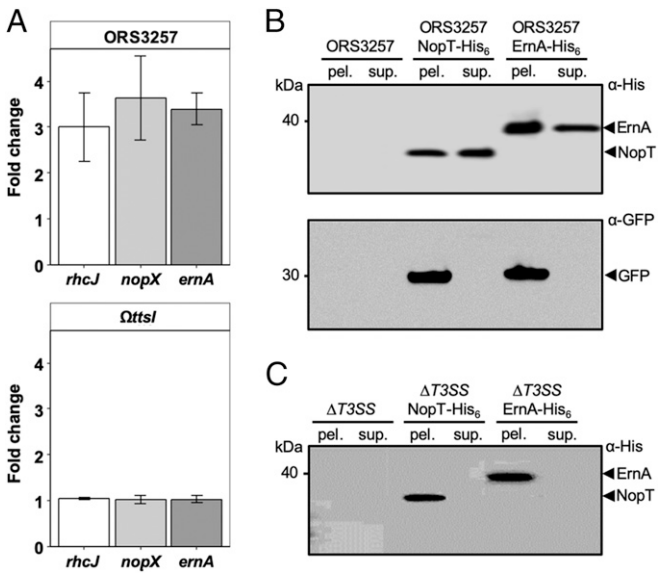

Fig. 2. The *ernA* gene encodes a bona fide T3E, and its expression is under the control of TtsI. (*A*) Fold change expression of *ernA* (*Brad3257_7701*) and 2 *T3SS* genes (*nopX* and *rhcJ*) used as controls in ORS3257 and the Ω*ttsI* mutant after induction with genistein. Bacteria cultivated in the absence of genistein but in presence of DMSO were used as reference. The expression levels were normalized using *adhB* (*Brad3257_3749*) transcripts. The level of expression was measured using qRT-PCR. Values represent mean ± SD ($n = 3$). (*B*) ErnA of ORS3257 is secreted in the supernatant. Secreted proteins from culture supernatants (sup.) or proteins from cell pellets (pel.) of the indicated strains were subjected to immunoblot analysis with the anti-His_6 (α-His) or anti-GFP (α-GFP) antibodies. (*C*) ErnA of ORS3257 is secreted via the T3SS. Secreted proteins from culture supernatants (sup.) or proteins from cell pellets (pel.) of the ORS3257Δ*T3SS* mutant strains were subjected to immunoblot analysis with the anti-His_6 antibody (α-His). The artifacts observed in panel *C* are not the result of an image treatment.

ErnA Homologs Are Widespread among Bradyrhizobia and Play a Key Role in *A. indica* Nodulation. Considering the importance of ErnA in the nodulation of *A. indica* and the fact that a diverse range of nonphotosynthetic *Bradyrhizobium* strains was found to induce the formation of a nodule-like structure on this plant (14), we investigated the prevalence of ErnA homologs among available bradyrhizobial genomes. Among the 148 sequenced *Bradyrhizobium* strains, 92 were found to possess a T3SS, among which 53, i.e., more than half, have a ErnA homolog (Fig. 3*A*). Conversely, no homolog was found in *Bradyrhizobium* strains without T3SS, nor in other genera of rhizobia, except for 3 T3SS-containing *Ensifer* strains (strains BJ1, TW10, and PC2) (*SI Appendix*, Fig. S6). This finding indicates that the *ernA* gene is widespread among the *Bradyrhizobium* strains with a T3SS and its presence is rather specific to this group. Notably, the ErnA amino acid sequences are highly conserved among these strains, with an identity ranging from 55 to 100% (*SI Appendix*, Fig. S6).

The high level of conservation of this effector in a wide range of bradyrhizobia prompted us to investigate whether ErnA effectors from other bradyrhizobia may also play a role in the establishment of the NF-independent, T3SS-dependent symbiosis. To test this hypothesis, we inactivated the corresponding gene (accession number LC460804, annotated $ernA_{61}$) in the *B. elkanii* USDA61 strain, which has been shown to nodulate *A. indica* in the absence of NF synthesis (14). As previously observed (14), the WT USDA61 strain induced a high number of uninfected nodules on *A. indica*, whereas the derived *T3SS* mutant (USDA61Ω*rhcJ*) had a strict Nod^- phenotype (Fig. 3*B*), thus confirming that the T3SS is required for nodule induction. The USDA61Ω$ernA_{61}$ mutant also displayed a nearly Nod^- phenotype (Fig. 3 *B* and *C*), similar to that observed with the *ernA* mutant of strain ORS3257 (Fig. 1 and *SI Appendix*, Fig. S5). These findings demonstrate that ErnA homologs found in other bradyrhizobia have a similar nodulation-conferring function during the symbiotic interaction with *A. indica*.

The Introduction of *ernA* Enables the *Bradyrhizobium* Strain DOA9 to Nodulate *A. indica*. To further demonstrate the importance of ErnA for nodule formation, we used a gain-of-function approach. For this purpose, we used the *Bradyrhizobium* DOA9 strain, which is unable to nodulate *Aeschynomene* species in an NF-independent manner (14, 22), despite the presence of a functional T3SS. Consistent with this nodulation defect, *ernA* was found to be missing in DOA9 (Fig. 3*A*).

To check whether ErnA could complement a nodulation-defective rhizobial strain, we introduced the *ernA* gene from ORS3257 ($ernA_{3257}$) into DOA9 and its *T3SS* mutant (DOA9Ω*rhcN*). As shown in Fig. 3 *B* and *C*, the DOA9::$ernA_{3257}$ strain was able to induce nodules on *A. indica* unlike the WT strain containing the empty vector (DOA9-pMG103) or the *T3SS* mutant strain expressing

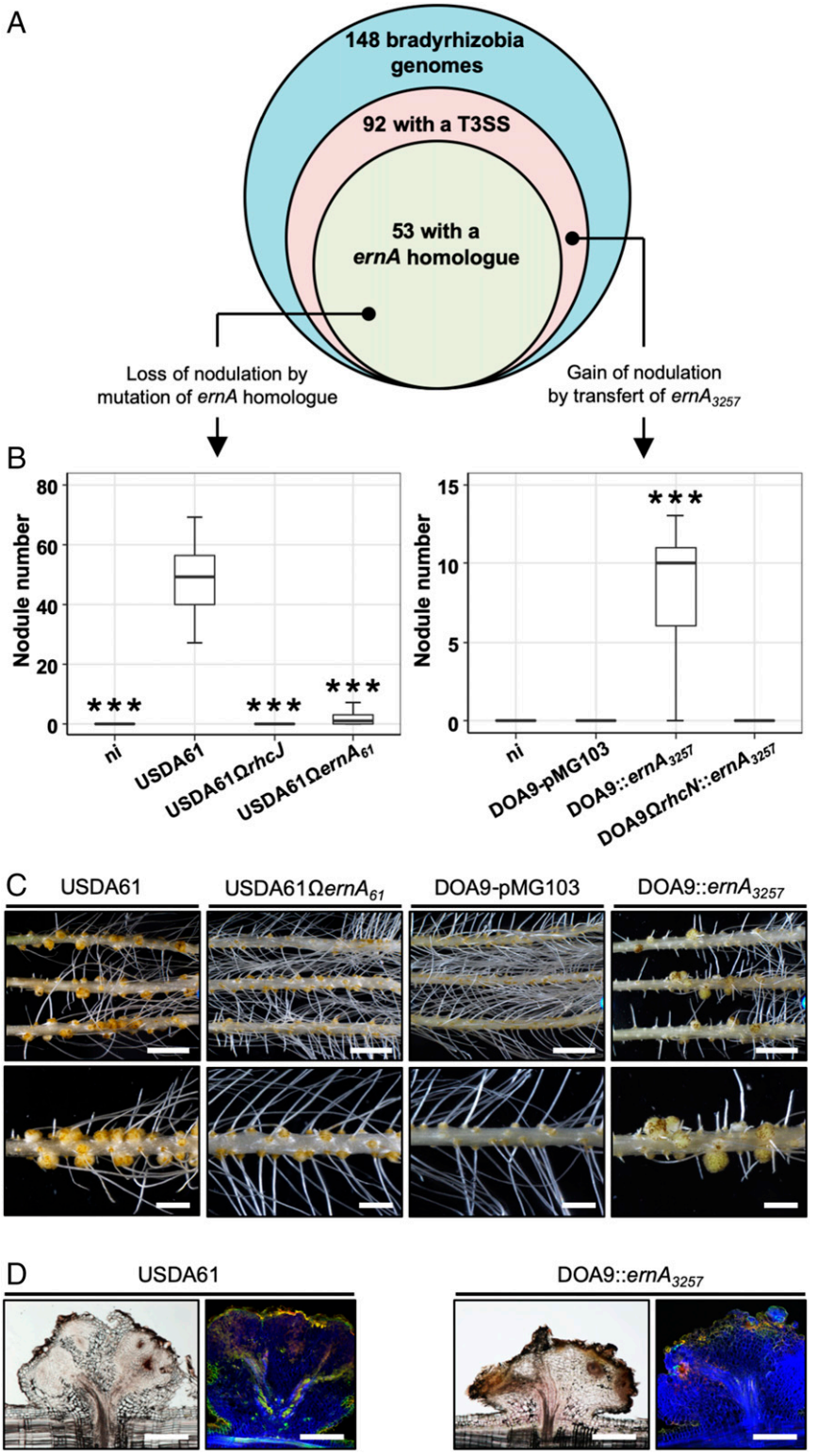

Fig. 3. Distribution of *ernA* genes among bradyrhizobia and symbiotic role in other strains after mutation or transfer. (*A*) Venn diagram representing the number of *Bradyrhizobium* strains with an available genome sequence and the proportion with a T3SS as well as a homolog of *ernA*. (*B–D*) Symbiotic properties on *A. indica* of 1) *B. elkanii* strain USDA61 and its mutant derivatives affected in the T3SS apparatus (USDA61Ω*rhcJ*) and the *ernA* homolog (USDA61Ω$ernA_{61}$), and 2) *Bradyrhizobium* sp. strain DOA9 derivatives (WT and the *T3SS* mutant DOA9Ω*rhcN*) containing the empty vector pMG103 or $ernA_{3257}$ cloned into pMG103. (*B*) Number of nodules formed on *A. indica* plants at 21 d after inoculation with the indicated strains. Box plots show results of 1 representative experiment out of at least 2 independent experiments per strain (18 plants each). The central rectangle spans the first quartile to the third quartile; the bold segment inside the rectangle shows the median; and the whiskers above and below the box show the locations of the maximum and minimum value, respectively. ***$P < 0.001$, significant differences between the WT strain and each mutant strain using a nonparametric Kruskal–Wallis test. (*C*) View of the roots and nodules elicited by the indicated strains. (Scale bars: *Upper*, 1.5 cm; *Lower*, 4 mm.) (*D*) Cytological analysis of the nodules elicited by the various strains tested. (Scale bars, 500 μm.)

ernA$_{3257}$ (DOA9Ω*rhcN*::*ernA*$_{3257}$). However, most of the nodules looked similar to those induced by the USDA61 strain, i.e., had no infected central tissue but did have some necrotic zones (Fig. 3*D*). These observations show that the introduction of *ernA* into DOA9 confers the ability to nodulate *A. indica*, but the symbiotic process remains incomplete, probably due to the presence of incompatibility factors and/or to the lack of certain factors that are needed to complete the infection process. Taken together, all these different experiments confirm that ErnA confers to bacteria the ability to form nodules on *Aeschynomene*.

ErnA Is Targeted to the Plant Nucleus. Alignment of the deduced amino acid sequences of ErnA homologs revealed the existence of 2 ErnA versions that differ in the presence or absence of an 80-amino acid domain at the N-terminal end of the protein (*SI Appendix*, Fig. S6). Both versions seem to play a similar role in triggering nodulation since mutation of the short (in strain ORS3257) and long form (in strain USDA61) led to the same Nod$^-$ phenotype in *A. indica*. A close examination of the 2 versions did not enable us to identify homology with known functional domains. However, a nuclear localization signal (NLS) present in the conserved N-terminal part of all ErnA homologs (*SI Appendix*, Fig. S6) was predicted using NLS mapper (23).

To investigate the subcellular localization of ErnA in plant cells, ErnA was C-terminally fused with enhanced GFP (ErnA-eGFP) and transiently expressed in *Nicotiana benthamiana* leaf cells upon *Agrobacterium tumefaciens*-mediated transformation. The GFP fluorescence was analyzed by laser-scanning confocal microscopy 48 h after infiltration. Consistent with the identification of a putative NLS motif, ErnA-eGFP was found to accumulate exclusively in the plant nucleus (Fig. 4*A*). The function of the NLS domain was verified by generating an ErnAΔNLS mutant C-terminally fused with eGFP (ErnAΔNLS-eGFP), which was found to display a nucleocytoplasmic distribution when transiently expressed in *N. benthamiana* cells (Fig. 4*A*). The fact that the ErnAΔNLS-eGFP version is still partially maintained in the nucleus might be explained by passive diffusion across the nucleus membrane given the relatively small size of the ErnA-eGFP protein (67 kDa).

Whether ErnA could also be targeted to the plant nucleus via secretion and injection through a T3SS was investigated using the GFP-strand complementation system that enables direct visualization of the bacterial delivery of effectors into host cells (24). Briefly, GFP is composed of 11 beta strands; when split into 2 parts consisting of strands 1 to 10 (GFP$_{1–10}$) and strand 11 (GFP$_{11}$), both (poly)peptide chains spontaneously reassemble into a functional GFP protein, provided that they are localized in the same cellular compartment. In this system, GFP$_{1–10}$ is constitutively expressed in stably transformed plant cells. When a bacterial effector tagged with the 11th strand of GFP (effector-GFP$_{11}$) is delivered *in planta*, GFP$_{1–10}$ and effector-GFP$_{11}$ reconstitute a fluorescent GFP molecule whose subcellular localization can be monitored. A construct containing ErnA fused with GFP$_{11}$ (ErnA-GFP$_{11}$) was introduced into *Pseudomonas fluorescens* (Pfo-1) cells, allowing T3SS-dependent delivery of the tagged effector. Twelve hours after infiltration of Pfo-1(*ernA-gfp$_{11}$*) cells into *Arabidopsis thaliana* Col-0 leaves constitutively expressing GFP$_{1–10}$, GFP fluorescence was detected in almost 90% of the observed host cell nuclei (Fig. 4*B*), confirming the localization deduced from the transient expression assay performed in *N. benthamiana* (Fig. 4*A*). As a negative control, when the ErnA effector lacking the GFP$_{11}$ (ErnA-3HA) was delivered by Pfo-1 cells in the GFP$_{1–10}$ transgenic line, no fluorescence could be detected (Fig. 4*B*). Collectively, these data demonstrate that the ErnA effector is translocated into the host cell and specifically targeted to the plant nucleus.

ErnA Binds Nucleic Acids in Plant Cell Nuclei. To better understand the mode of action of ErnA in the nucleus, we investigated whether it can interact with nuclear nucleic acids. To this end, we performed a FRET-FLIM (fluorescence resonance energy transfer with fluorescence lifetime imaging microscopy) assay dedicated to the detection of protein–nucleic acid interactions *in planta* (25). The nuclear targeted ErnA-eGFP fusion protein (Fig. 4*A*) was used as the donor fluorophore. Nuclear nucleic acids were converted into FRET acceptors with a DNA-binding fluorescent dye (SYTOX Orange). In the absence of SYTOX Orange treatment, an average GFP lifetime of 2.30 ns was measured (Fig. 4*C* and *SI Appendix*, Table S3). A significant decrease in the ErnA-eGFP lifetime was observed (1.94 ns) in SYTOX Orange-treated samples due to FRET, indicating a close association between the ErnA-eGFP partner (donor) and the stained nuclear nucleic acids (acceptor) (Fig. 4*C* and *SI Appendix*, Table S3). To verify that the detection of such FRET was not due to the overaccumulation of ErnA-eGFP in SYTOX Orange-stained nuclei, we used as a negative control a variant of the *Arabidopsis* RRS1 immune receptor (RRS1-KR) whose ability to interact with DNA is abolished by a mutation in its DNA-binding domain (26). As expected, no FRET could be detected in SYTOX-treated leaf samples expressing RRS1-KR-eGFP (*SI Appendix*, Table S3). Together, these data support the idea that ErnA-eGFP is closely associated with nucleic acids in the plant nucleus.

The Ectopic Expression of ErnA in *A. indica* Roots Activates Organogenesis of Root- and Nodule-Like Structures. In order to obtain further evidence for the ability of ErnA to trigger nodule organogenesis, transgenic hairy root lines of *A. indica* overexpressing *ernA* under the control of the 35S promoter and expressing DsRed as a marker for transformation were generated and grown in the absence of bradyrhizobia. The production of the effector was verified by immunoblot analysis with an ErnA-specific antibody (α-ErnA) (*SI Appendix*, Fig. S7). As early as 3 wk after transformation, some roots expressing *ernA* displayed a succession of small bumps highlighted by strong DsRed fluorescence (Fig. 5*B*). After 7 wk of growth, a pronounced change in the root architecture was observed in 105 out of 135 *ernA*-overexpressing plants. This change was characterized by a large number of closely spaced swellings or protrusions all along the apical–basal axis of the root (Fig. 5 *C* and *D*). In root sections, 2 different types of protrusions were distinguishable. In the first type, the protrusions looked like emerging lateral roots whose development was interrupted (Fig. 5 *E–H*). This type of protrusion was located all around the transformed roots and contained central vascularization (Fig. 5*H*). In rare cases, new meristems were visible all along these lateral root-like structures (Fig. 5*I*). The second type of protrusion resembled nodule primordia (Fig. 5 *J–N*). These protrusions were generally located on one side of the root and were often associated with an accumulation of brownish compounds, suggesting the occurrence of a plant defense response (Fig. 5 *J* and *K*). These protrusions were also more round in shape and were associated with central tissue composed of small dividing cells (Fig. 5 *L–N*). Occasionally, large tumor-like structures were also observed on plants overexpressing *ernA* (Fig. 5 *O* and *P*). Staining the nuclei with propidium iodide revealed that the structures were composed of an agglomeration of meristems (Fig. 5*P*). None of these phenotypes were observed in the 93 plants that were transformed with the empty vector (Fig. 5*A*). Altogether, these results demonstrate that, in the absence of bradyrhizobia, ErnA alone is capable of inducing cell divisions, ultimately leading to the initiation of new meristems.

Discussion

The knowledge that certain bradyrhizobia can activate the nodulation process in some legume plants in the absence of NF signaling but in a T3SS-dependent manner has only recently emerged (13, 14). Here, we significantly advanced our understanding

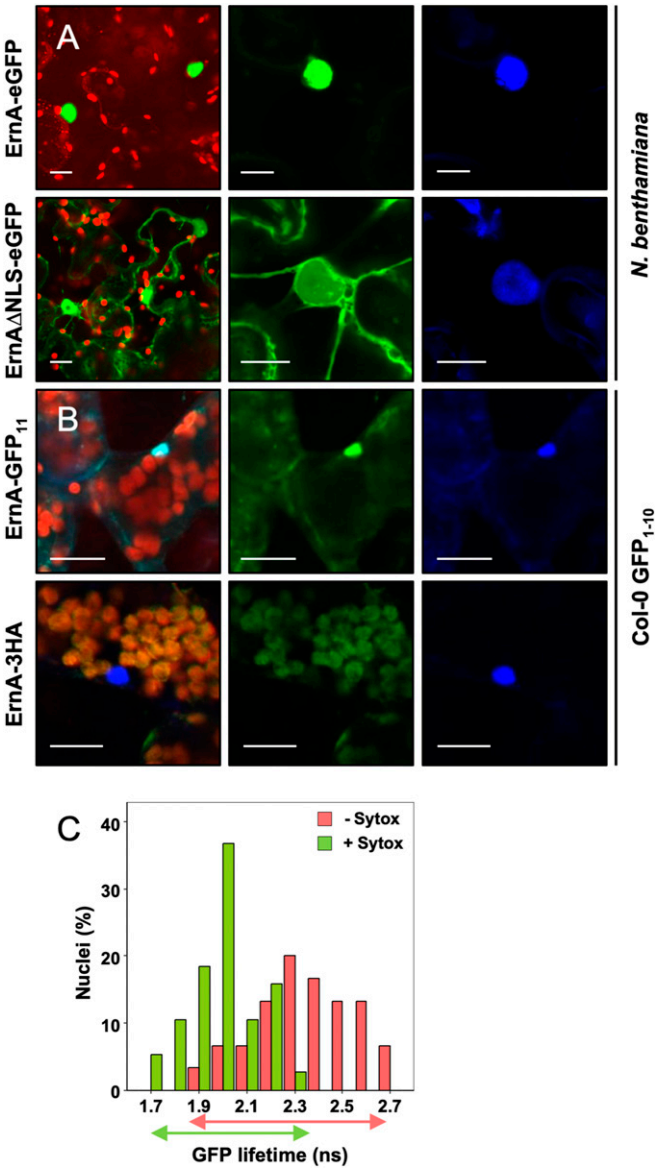

Fig. 4. ErnA is targeted to the plant cell nucleus and interacts with nucleic acids. (*A*) GFP fluorescence observed in *N. benthamiana* leaves transiently expressing ErnA-eGFP or ErnAΔNLS-eGFP. GFP was visualized by confocal microscopy 48 h after *Agrobacterium* infiltration of the leaves. From *Left* to *Right*: an overlay of GFP and chlorophyll fluorescence from transformed leaf cells, and the GFP and DAPI fluorescence spectrum of a representative nucleus from a transformed cell. Staining with DAPI was used to visualize nuclei. At least 10 nuclei were observed, and all of them showed the same distribution pattern of DAPI staining and GFP fluorescence. (Scale bars, 15 μm.) (*B*) Visualization of ErnA-GFP_{11} in *Arabidopsis* cells after its secretion and injection by *P. fluorescens*. Three-week-old *Arabidopsis* Col-0 plants expressing $GFP_{1–10}$ were infiltrated with *P. fluorescens* expressing either ErnA-GFP_{11} or ErnA-3HA. Reconstituted GFP was visualized by confocal microscopy 12 h postinfiltration. From *Left* to *Right*: an overlay of GFP, DAPI, and chlorophyll fluorescence spectrum, and the GFP and DAPI fluorescence spectrum, respectively. Staining with DAPI was used to visualize nuclei. (Scale bars, 15 μm.) (*C*) GFP lifetime distribution of nuclear ErnA-eGFP in presence or in absence of SYTOX Orange. FRET-FLIM measurements (*SI Appendix*, Table S3) were performed as described in *Methods*. Histograms show the distribution of nuclei (in percentage) according to classes of GFP lifetime value (in nanoseconds) in the absence (red bars) or in the presence (green bars) of the SYTOX Orange acceptor. The measured lifetimes of ErnA-eGFP were clearly shifted to lower values in the presence of SYTOX Orange compared to samples without the acceptor (indicated by partial overlap between green and orange arrows spanning relative GFP lifetime classes).

of this alternative symbiotic process by showing that it relies on a subtle mixture of at least 5 effectors playing synergistic and complementary roles (Fig. 6). The effectors NopM1 and NopP1 most probably act together to suppress the plant immune responses and are required to maintain a chronic intracellular infection. The NopAB and NopT effectors appear to play a role in early steps of the symbiotic process and are required for efficient nodule infection. Finally, we identified the effector ErnA as a key factor to form nodules.

Three of these 5 effectors (NopM1, NopP1, and NopT) have already been characterized in other rhizobia. NopM and NopP play a positive role during the interaction between *Ensifer fredii* NGR234 and several legumes species, as mutants in these genes induced fewer nodules (20, 27). Both are thought to suppress plant defense reactions. NopM, which has an E3 ubiquitin ligase domain, reduces the production of flagellin elicitor-induced reactive oxygen species when transiently expressed in *N. benthamiana* (19). NopP is phosphorylated by plant kinases, but so far it is not known whether this phosphorylation interferes with plant defense signaling (18). NopT also plays a positive role in *E. fredii* NGR234 during the interaction with *Phaseolus vulgaris* and *Tephrosia vogelii* (28). NopT effectors are cysteine proteases belonging to the YopT-AvrPphB effector family, which localize at the cytoplasmic membrane of the host cell, but their modes of action remain unknown. Interestingly, the NopT homolog in *Yersinia pestis*, named YopT, has been reported to affect the actin cytoskeleton of the host cell by modulating the function of Rho GTPases (29). Considering that assembly of actin filament networks is critical during the endocytotic uptake of rhizobia in symbiosomes (30), NopT probably plays a direct role in the infection process. The 2 other effectors, NopAB and ErnA, have never been reported to play a symbiotic role even though both have homologs in a diverse range of bradyrhizobia. The NopAB and ErnA effectors do not show homology with known functional domains.

Here, we provide evidence that ErnA localizes in the host nucleus and binds nucleic acids. From these data, it is tempting to hypothesize that ErnA associates with nuclear nucleic acids to manipulate host gene expression. Further experiments are necessary to determine whether the function of ErnA depends on this nuclear localization and whether its nucleic acid binding properties are linked with transcriptional programming. Interestingly, transformed roots of *A. indica* expressing ErnA displayed numerous meristem-like structures all along the root, a phenotype reminiscent of the one observed in *Arabidopsis* root explants grown on medium containing auxin (31). It is therefore possible that ErnA positively influences plant cell division by modulating the cytokinin/auxin balance, 2 key phytohormones governing nodule and root meristem induction (32). Interestingly, similar structures have also been observed in *Lotus japonicus* overexpressing the NIN or NF-Y transcription factors, which are key components of the NF signaling pathway controlling nodule organogenesis (33, 34). However, the nature of the organs induced by the expression of *ernA* remains unclear, and the question whether ErnA-mediated organogenesis activates the common symbiosis signaling pathway needs to be addressed.

To our knowledge, ErnA is the only rhizobial effector reported to play a direct role in nodule development. Interestingly, a parallel can be drawn with some pathogenic T3Es reported to induce gall formation, such as HsvG or HsvB identified in *Pantoea agglomerans* or to induce cytokinin signaling such as the *Pseudomonas syringae* HopQ1 effector (35, 36). To better understand the mode of

Values were obtained from 8 different foliar discs collected 48 h postinfection and obtained from 2 independent experiments. Notably, upon transient expression of *ernA* in *N. benthamiana* leaves, no callus development or any other morphological changes were observed.

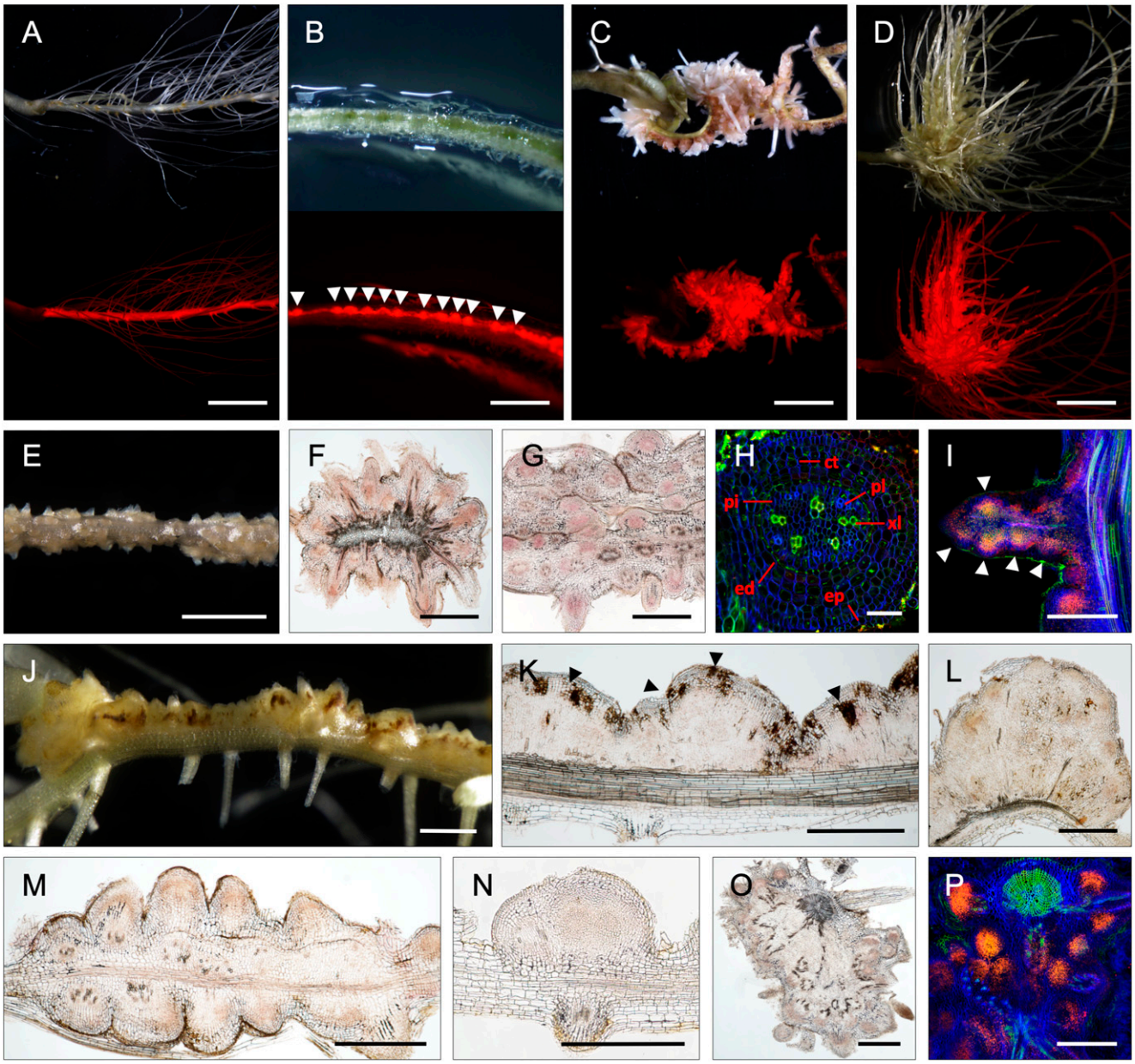

Fig. 5. ErnA induces meristematic protuberances. (*A–D*) *A. indica* roots transformed with either the empty vector containing the DsRed marker (*A*) or *p35S-ernA* (*B–D*) and observed by a light (*Upper*) or a fluorescent (*Lower*) stereomicroscope equipped with a DsRed filter. Observations were made at 3 wk (*B*) or 7 wk (*A*, *C*, and *D*) after transformation in the absence of bradyrhizobia. White arrowheads in *B* indicate the formation of small bumps. (*E–I*) Lateral root-like structures induced by *p35S-ernA* observed 7 wk after transformation. View of lateral root-like structures (*E*). Cross-sections of transformed roots forming lateral root-like structures (*F* and *G*). (*H* and *I*) Confocal microscopy of lateral root-like structures using staining with SYTO 9 (green; xylem vessels), calcofluor (blue; plant cell wall), and propidium iodide (red; plant nuclei). In *H*, abbreviations: ct, cortical cells; ed, endoderm; ep, epiderm; pi, pericycle; pl, phloem; xl, xylem vessels. In *I*, white arrowheads indicate new meristems. (*J–N*) Root nodule-like primordia structures induced by p35S-*ernA*. View of the root nodule-like primordia (*J*). Longitudinal sections of root nodule-like primordia (*K–N*). In *K*, black arrowheads indicate necrotic zones. (*O* and *P*) Cross-sections of tumor-like structures observed either by light (*O*) or by confocal microscopy (*P*) after staining as in *H* and *I*. (Scale bars: *A*, *C*, and *D*, 1.5 cm; *B*, *E*, and *J*, 2 mm; *F*, *G*, *I*, and *K–P*, 500 μm; *H*, 50 μm.)

action of ErnA, our next challenge is to identify its target(s) and to investigate whether there is a link between ErnA and the NF-dependent signaling pathway.

The key role of ErnA in nodule formation is strengthened by the observation that the 2 *ernA* mutants in USDA61 and ORS3257 strains lost their ability to nodulate *A. indica*. Moreover, introducing *ernA* in the nodulation-defective *Bradyrhizobium* strain DOA9 made it capable of inducing nodules. It should be noted that several *Bradyrhizobium* strains containing *ernA*, such as *B. diazoefficiens* USDA110, and USDA122, and *B. japonicum* USDA124, are unable to induce nodules on *A. indica* (14). This suggests that, besides ErnA, other factors have to act in concert to establish NF-independent, T3SS-dependent nodulation. Moreover, we cannot exclude the possibility that these strains deliver effectors that activate host immune responses, thereby rendering the interaction incompatible. Finally, it is possible that despite the high conservation of the proteins in the bradyrhizobia, some ErnA variants have different nodule-inducing abilities.

In most bradyrhizobia, the *T3SS* gene cluster colocalizes with the *nod* gene cluster. This indicates that the T3SS is an integral

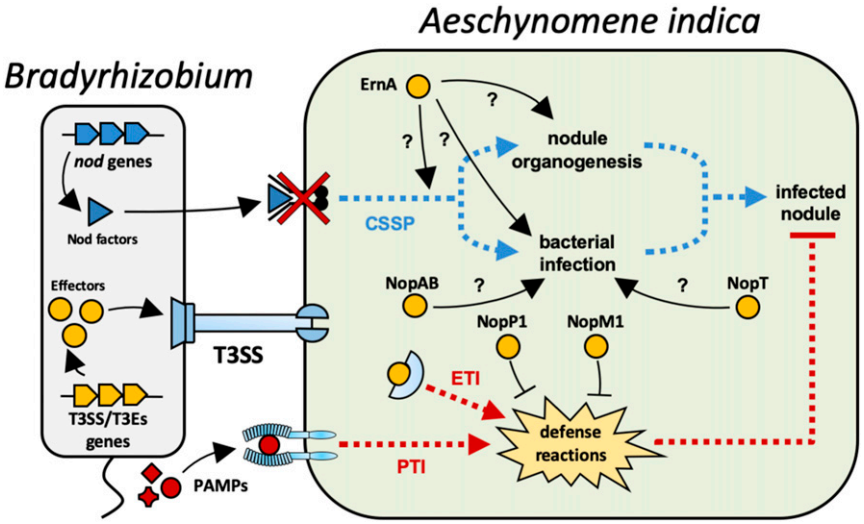

Fig. 6. Proposed model for the NF-independent, T3SS-dependent symbiotic process between *Bradyrhizobium* ORS3257 and *A. indica*. The symbiosis between ORS3257 and *A. indica* does not involve NFs but depends on a mixture of T3Es delivered into the host cell where they act in concert for nodulation. NopP1 and NopM1 suppress plant defense responses resulting from the activation of PTI and/or ETI. Both NopAB and NopT effectors promote bacterial infection of the nodule, directly or indirectly. The ErnA effector triggers organ development either by activating the common symbiosis signaling pathway (CSSP) or by a yet-unknown mechanism. Moreover, we cannot exclude that ErnA is also involved, directly or indirectly, in the infection process.

part of the arsenal of tools available to the bacteria to enable a symbiotic interaction with legumes. Until now, this T3SS machinery was viewed as accessory equipment that modulates the host spectrum of the bacteria by interfering with plant immune responses. The discovery that a single effector protein, widely distributed among bradyrhizobia, is capable of inducing nodule organogenesis, suggests that legume nodulation programs, which until now were considered to be under the (almost) exclusive control of NFs and the common symbiosis signaling pathway, can also be regulated by T3SS effectors in a wide range of rhizobium–legume interactions. This is a major breakthrough in the field that could pave the way for designing strategies to transfer nodulation to nonleguminous plants.

Methods

Bacterial Strains and Growth Conditions. *Bradyrhizobium* strains ORS3257, DOA9, and USDA61 and their derivatives (*SI Appendix*, Table S4) were grown in yeast mannitol medium (37) at 34 °C. *Escherichia coli* strains were grown at 37 °C in Luria–Bertani (LB) medium (38). *Agrobacterium rhizogenes* Arqua1 and *A. tumefaciens* GV3101 were grown at 28 °C in arabinose–gluconate medium (39) and *P. fluorescens* was grown in King's B medium (40). When required, the media were supplemented with the appropriate antibiotics at the following concentrations: 50 μg/mL kanamycin, 20 μg/mL nalidixic acid, 20 μg/mL cefotaxime (Cefo), and 100 μg/mL spectinomycin.

Plasmid Construction, Mutagenesis, and Complementation. Standard molecular biology techniques were used for all cloning procedures. All constructions made in this study are listed in *SI Appendix*, Table S4, which also includes the primers and the cloning strategies. For the construction of insertional mutants (obtained by single crossing-over), a 250- to 350-bp internal fragment of the target gene was amplified by PCR and cloned into the nonreplicative plasmid pVO155-npt2-GFP-npt2-Cefo (14). For the construction of deletion mutants (obtained by double crossing-over), 750- to 1,000-bp PCR fragments corresponding to the upstream and downstream flanking regions of the locus of interest were merged by overlap extension PCR and cloned into pNPTS129, which carries the *sacB* gene (41). Subsequently, a Cefo resistance cassette was introduced between the upstream and downstream flanking regions previously cloned into the pNPTS129 plasmid. The resulting plasmids were then transferred by conjugation into *Bradyrhizobium* strains as described previously (42). Single recombinant mutants were obtained by growing the bacteria on plates containing a selective antibiotic and subsequently verified by diagnostic PCR. Deletion mutants were selected in a subsequent step in which bacteria were grown on sucrose–Cefo plates. Sucrose- and Cefo-resistant clones were checked for loss of kanamycin resistance from the pNPTS129 plasmid, and kanamycin-sensitive clones were screened by PCR for the deletion of the corresponding genomic DNA region.

For complementation experiments of the ORS3257Δ*7701* mutant, a PCR fragment encompassing the *Brad3257_7701* gene including the 500-bp upstream promoter region was cloned into pVO155-npt2-GFP (14) and reintroduced into the Δ*7701* mutant by single crossing-over. The same DNA region was also cloned into pMG103-npt2-cefo-npt2-GFP and transferred into DOA9 by electroporation as previously described (43).

Plant Cultivation and Symbiotic Analysis. *A. indica* plants were grown and inoculated as previously described (14). Eighteen plants per condition were taken at 21 d postinoculation for nodulation and nitrogen fixation assays, and the number of nodules and nitrogenase activity were analyzed as previously described (44). The experiments were carried out at least in duplicate. For microscopic analysis, nodules and transformed roots were harvested and observed directly or upon embedding in agarose (4%), and then freshly sliced into 30-μm sections with a Leica VT1200S vibratome (Leica Microsystems). The nodule sections were incubated for 15 min in live/dead staining solution (LIVE/DEAD BacLight Bacterial Viability Kit; Molecular Probes) and then analyzed as previously described (14).

Expression Analyses. *Bradyrhizobium* WT strain ORS3257 and its Ω*ttsI* mutant were cultivated in BNM-B minimal medium (45). When the OD_{600} reached ~0.4, 5 μM genistein dissolved in DMSO or DMSO alone was added, and the cultures were harvested after 24 h. Total RNA was extracted using the Ribopure Bacteria kit (Ambion) and treated with DNase I (Qiagen). One hundred nanograms of total RNA per sample were reverse transcribed using SuperScript II reverse transcriptase (Invitrogen) and random hexamer primers, following the supplier's protocol. Real-time qPCR was performed using the Brilliant III Ultra-Fast SYBR Green QPCR Master Mix (Agilent Technologies). Transcript levels were normalized to the expression of the *adhB* gene (*Brad3257_3749*). Primers used to amplify *adhB*, *rhcN*, *nopX*, and *ernA* transcripts are listed in *SI Appendix*, Table S5.

Production of Anti-ErnA Antibody. An *E. coli* BL21 strain expressing His_6-tagged ErnA from strain ORS3257 was constructed. A PCR fragment of the *ernA* gene from the start to the last codon before the stop was amplified using a reverse primer containing an in-frame His_6-tag sequence and a stop codon. The PCR product was cloned into the pET-29b vector (Merck) (*SI Appendix*, Table S4), and the resulting construct was introduced in the *E. coli* strain BL21.

The *E. coli* BL21 ErnA-His_6 strain was grown for 3 h at 37 °C in LB medium supplemented with 5 mM IPTG to induce the expression of the ErnA-His_6 protein. Cells were harvested by centrifugation, resuspended in 50 mM Tris·HCl, pH 8.0, 20 mM imidazole, 500 mM NaCl buffer, and disrupted by sonication. After centrifugation at 20,000 × *g* at 4 °C for 30 min, His_6-tagged

protein was purified as described by Marty et al. (46). Purified protein was used for the production of rabbit polyclonal antibodies (Agro-Bio). Two rabbits were immunized by injecting 1 mg of purified protein and exsanguinated after 42 d to collect antiserum.

Immunoblot Analysis. Six hundred milliliters of BNM-B minimal medium were inoculated with 3-mL precultures of the ORS3257 and Δ*T3SS* strains containing a His_6-tagged version of *ernA* or *nopT* (see *SI Appendix*, Table S4 for the constructions). Bacteria were cultivated at 28 °C for 48 h in the presence of genistein (5 μM) at 200 rpm. To prepare proteins from the culture supernatant, bacterial cells and exopolysaccharides were separated from the supernatant in 2 centrifugation steps (first step: 1 h, 4,000 × *g*, 4 °C; second step: 30 min, 8,000 × *g*, 4 °C). Proteins in the supernatant were precipitated using trichloroacetic acid as previously described (47) and resuspended in 75 μL of NuPAGE LDS Sample Buffer (#NP0007; Thermo Fisher) for SDS/PAGE analysis. For analysis of cellular proteins, bacterial cells were resuspended in 5 mL of solubilization buffer (50 mM Tris·HCl, pH 8.0, 20 mM imidazole, and 300 mM NaCl) and lysed by 5 freeze–thaw cycles in liquid nitrogen. After centrifugation (30 min, 8,000 × *g*, 4 °C), 4× LDS Sample Buffer was added to the supernatant corresponding to the soluble proteins of the cell. Protein solutions (25 μL) from bacterial cells and culture supernatants were separated on 12.5% SDS/PAGE gels and transferred to polyvinylidene difluoride membranes. The membranes were then blocked for 1 h in PBSTM buffer (PBS, 0.1% Tween 20, 5% nonfat milk). The appropriate antibodies were added to the PBSTM and the membranes were incubated for 2 h at room temperature. Mouse antibodies were used at the following dilutions: anti–His_6-tag (#SAB1305538; Merck), 1:1,000, and anti-GFP (#SAB4200681; Merck), 1:2,000. The membranes were then incubated for 2 h with peroxidase-conjugated anti-mouse IgGs (1:500; #A9044; Merck). Immunoblotted proteins were detected by chemiluminescence using the Pierce ECL Plus Western Blotting Substrate (#32132; Thermo Fisher) according to the manufacturer's protocols.

To confirm expression of *ernA* in transformed roots of *Aeschynomene*, total protein extracts from 200 mg of roots were obtained using the Plant Total Protein Extraction Kit (#PE0230; Sigma-Aldrich) according to the manufacturer's protocols. Approximately 10 mg of protein were used for Western blot analysis as described above using the anti-ErnA antibody diluted at 1:1,000 and an anti-rabbit antibody (/#AP132P; Merck) diluted at 1:500.

Effector Delivery in *Arabidopsis thaliana*. The *ernA-gfp*$_{11}$ DNA fragment constructed as described in *SI Appendix*, Table S4, was cloned into the pBBR-GWY-3HA (26) destination vector, thus allowing the expression of *ernA-gfp*$_{11}$ in *Pseudomonas fluorescens* (*Pfo-1*) cells. The effector delivery assay using syringe infiltration was performed on 3-wk-old plants of *Arabidopsis* Col-0 *GFP*$_{1-10}$ using *Pfo-1*(*ernA-gfp*$_{11}$) cells resuspended in 10 mM $MgCl_2$ (OD_{600} = 0.2). Discs (6 mm) of infiltrated leaves were collected 12 h post-inoculation, mounted on a glass slide, and covered with a coverslip. Images were acquired with a confocal microscope (Leica; SP2 AOBS) using a 40× water-immersion lens (numerical aperture [N.A.] 0.8). For excitation, a 405-nm ray line of a diode laser and the 488-nm ray line of an argon laser were used and the emitted fluorescence collected in the blue range between 410 and 470 nm and in the green range between 500 and 530 nm.

***Agrobacterium tumefaciens* Infiltration Assays in *Nicotiana benthamiana*.** Plasmid *p35S-ernA-gfp* expressing ErnA-eGFP under the control of the 35S promoter (*SI Appendix*, Table S4) was introduced into *A. tumefaciens* strain GV3101 by electroporation (48). Leaves from 4-wk-old *N. benthamiana* plants were infiltrated using a needleless syringe containing bacteria resuspended in infiltration buffer (10 mM $MgCl_2$; 10 mM MES-KOH, pH 5.6; 150 μM acetosyringone) and adjusted to OD_{600} = 0.5.

After 48 h following *A. tumefaciens* infiltration, *N. benthamiana* leaf samples were incubated in 5 μg/mL DAPI solution (4′,6-diamidino-2-phenylindole; Sigma) for 30 min. Localization of fluorescently labeled ErnA was observed with a confocal microscope (Leica SP2 AOBS) using the 488-nm ray line of an argon laser for excitation, the green (GFP) and the blue (DAPI) emitted fluorescence being collected between 510/550 nm and 410/470 nm, respectively.

Preparation of Leaf Samples for FRET-FLIM Assays. Leaf samples were prepared as previously described (26). *A. tumefaciens*-infiltrated *N. benthamiana* leaf disk samples (8 mm in diameter, harvested 48 h after infiltration) were vacuum-infiltrated with a TBS buffer (Tris·HCl, 25 mM, pH 7.5; NaCl, 140 mM; KCl, 3 mM) containing 4% (wt/vol) paraformaldehyde and incubated for 20 min at 4 °C. The fixed samples were permeabilized by incubation in proteinase K solution (Tris·HCl, 50 mM, pH 7.5; NaCl, 100 mM; EDTA, 1 mM; SDS, 0.5%; 200 μg/mL of proteinase K [Invitrogen]) for 10 min at 37 °C. Nucleic acid staining was performed by vacuum-infiltrating a 5 μM SYTOX Orange (Invitrogen) solution in TBS buffer and incubating samples for 30 min at room temperature in the dark. Fixed leaf discs were washed with and mounted on TBS buffer before observations on an inverted microscope (Eclipse TE2000E; Nikon).

FRET-FLIM Measurements. Fluorescence lifetime measurements were performed with a FLIM system based on a time domain approach using a streak camera, as previously described (26). The light source was a laser picosecond pulse source (PLP 481 nm, pulse duration of 70 ps, 340-mW peak pulse power; Hamamatsu Photonics) with a fundamental frequency of 20 MHz. All images were acquired with a 60× oil-immersion lens (Plan APO, 1.4 N.A., IR) mounted on an inverted microscope (Eclipse TE2000E; Nikon). The pulse laser emission was directed back into the detection unit through a dichroic mirror (495/25 nm) and a bandpass filter (520/25 nm). The detector was a 20-MHz streak camera (Streakscope C10627; Hamamatsu Photonics) coupled to a fast and high-sensitivity CCD camera (model C8800-53C; Hamamatsu Photonics). For each nucleus, average fluorescence decay profiles were plotted and lifetimes were estimated by fitting data with exponential function using a nonlinear least-squares estimation procedure (25). Fluorescence lifetime of the donor (GFP) was experimentally measured in the presence and absence of the acceptor (SYTOX Orange). FRET efficiency (E) was calculated by comparing the lifetime of the donor in the presence (τ_{DA}) or absence (τ_D) of the acceptor: $E = 1 - (\tau_{DA})/(\tau_D)$. Statistical comparisons between control (donor) and assay (donor + acceptor) lifetime values were performed by Student's *t* test. For each experiment, 8 leaf discs obtained from 4 *A. tumefaciens*-infiltrated leaves were used to collect data.

Hairy Root Transformation with *Agrobacterium rhizogenes*. Plasmid p35S-*ernA* containing *ernA* under the control of the 35S promoter (see *SI Appendix*, Table S4, for the construction) and the empty vector pJCV51 with the DsRed marker (https://gateway.psb.ugent.be) were introduced by electroporation into the *A. rhizogenes* ARqua1 strain used for hairy root transformations. *A. indica* roots were transformed following previously described procedures (39). The plant roots were observed at 3 and 7 wk posttransformation.

ACKNOWLEDGMENTS. We thank Dr. Gitta Coaker for providing the Col-0 35S-GFP_{1-10} plants. This work was supported by grants from the French National Research Agency (Grant "SymEffectors"; ANR-16-CE20-0013) and from the Franco-Japanese Cooperation Program (Partenariat Hubert Curien SAKURA 2017; Grant 35920RL). L.D. is supported by the ANR Project RADAR (ANR15-CE20-0016-01) and the French Laboratory of Excellence Project TULIP (ANR-10-LABX-41; ANR-11-IDEX-0002-02). A.T. was supported by a PhD fellowship from the French Ministry of National Education, Higher Education and Research.

1. P. Lerouge *et al.*, Symbiotic host-specificity of *Rhizobium meliloti* is determined by a sulphated and acylated glucosamine oligosaccharide signal. *Nature* **344**, 781–784 (1990).
2. G. E. Oldroyd, J. D. Murray, P. S. Poole, J. A. Downie, The rules of engagement in the legume-rhizobial symbiosis. *Annu. Rev. Genet.* **45**, 119–144 (2011).
3. F. Berrabah, P. Ratet, B. Gourion, Legume nodules: Massive infection in the absence of defense induction. *Mol. Plant Microbe Interact.* **32**, 35–44 (2019).
4. B. Gourion, F. Berrabah, P. Ratet, G. Stacey, Rhizobium-legume symbioses: The crucial role of plant immunity. *Trends Plant Sci.* **20**, 186–194 (2015).
5. Y. Cao, M. K. Halane, W. Gassmann, G. Stacey, The role of plant innate immunity in the legume-rhizobium symbiosis. *Annu. Rev. Plant Biol.* **68**, 535–561 (2017).
6. W. J. Deakin, W. J. Broughton, Symbiotic use of pathogenic strategies: Rhizobial protein secretion systems. *Nat. Rev. Microbiol.* **7**, 312–320 (2009).
7. R. Q. Notti, C. E. Stebbins, The structure and function of type III secretion systems. *Microbiol. Spectr.* **4**, VMBF-0004-2015 (2016).
8. A. P. Tampakaki, Commonalities and differences of T3SSs in rhizobia and plant pathogenic bacteria. *Front. Plant Sci.* **5**, 114 (2014).
9. C. Staehelin, H. B. Krishnan, Nodulation outer proteins: Double-edged swords of symbiotic rhizobia. *Biochem. J.* **470**, 263–274 (2015).
10. H. Miwa, S. Okazaki, How effectors promote beneficial interactions. *Curr. Opin. Plant Biol.* **38**, 148–154 (2017).
11. S. Yang, F. Tang, M. Gao, H. B. Krishnan, H. Zhu, *R* gene-controlled host specificity in the legume-rhizobia symbiosis. *Proc. Natl. Acad. Sci. U.S.A.* **107**, 18735–18740 (2010).
12. M. Sugawara *et al.*, Variation in bradyrhizobial NopP effector determines symbiotic incompatibility with Rj2-soybeans via effector-triggered immunity. *Nat. Commun.* **9**, 3139 (2018).
13. S. Okazaki, T. Kaneko, S. Sato, K. Saeki, Hijacking of leguminous nodulation signaling by the rhizobial type III secretion system. *Proc. Natl. Acad. Sci. U.S.A.* **110**, 17131–17136 (2013).
14. S. Okazaki *et al.*, Rhizobium-legume symbiosis in the absence of Nod factors: Two possible scenarios with or without the T3SS. *ISME J.* **10**, 64–74 (2016).
15. E. Giraud *et al.*, Legumes symbioses: Absence of *Nod* genes in photosynthetic bradyrhizobia. *Science* **316**, 1307–1312 (2007).

16. A. Krause, A. Doerfel, M. Göttfert, Mutational and transcriptional analysis of the type III secretion system of *Bradyrhizobium japonicum*. *Mol. Plant Microbe Interact.* **15**, 1228–1235 (2002).
17. R. Wassem *et al*., TtsI regulates symbiotic genes in *Rhizobium* species NGR234 by binding to *tts* boxes. *Mol. Microbiol.* **68**, 736–748 (2008).
18. P. Skorpil *et al*., NopP, a phosphorylated effector of *Rhizobium* sp. strain NGR234, is a major determinant of nodulation of the tropical legumes *Flemingia congesta* and *Tephrosia vogelii*. *Mol. Microbiol.* **57**, 1304–1317 (2005).
19. D. W. Xin *et al*., Functional analysis of NopM, a novel E3 ubiquitin ligase (NEL) domain effector of *Rhizobium* sp. strain NGR234. *PLoS Pathog.* **8**, e1002707 (2012).
20. K. Kambara *et al*., Rhizobia utilize pathogen-like effector proteins during symbiosis. *Mol. Microbiol.* **71**, 92–106 (2009).
21. J. Hempel, S. Zehner, M. Göttfert, T. Patschkowski, Analysis of the secretome of the soybean symbiont *Bradyrhizobium japonicum*. *J. Biotechnol.* **140**, 51–58 (2009).
22. R. Noisangiam *et al*., Genetic diversity, symbiotic evolution, and proposed infection process of *Bradyrhizobium* strains isolated from root nodules of *Aeschynomene americana* L. in Thailand. *Appl. Environ. Microbiol.* **78**, 6236–6250 (2012).
23. S. Kosugi, M. Hasebe, M. Tomita, H. Yanagawa, Systematic identification of cell cycle-dependent yeast nucleocytoplasmic shuttling proteins by prediction of composite motifs. *Proc. Natl. Acad. Sci. U.S.A.* **106**, 10171–10176 (2009). Correction in: *Proc. Natl. Acad. Sci. U.S.A.* 106, 13142 (2009).
24. E. Henry, T. Y. Toruño, A. Jauneau, L. Deslandes, G. Coaker, Direct and indirect visualization of bacterial effector delivery into diverse plant cell types during infection. *Plant Cell* **29**, 1555–1570 (2017).
25. L. Camborde *et al*., Detection of nucleic acid-protein interactions in plant leaves using fluorescence lifetime imaging microscopy. *Nat. Protoc.* **12**, 1933–1950 (2017).
26. C. Le Roux *et al*., A receptor pair with an integrated decoy converts pathogen disabling of transcription factors to immunity. *Cell* **161**, 1074–1088 (2015).
27. C. Marie *et al*., Characterization of Nops, nodulation outer proteins, secreted via the type III secretion system of NGR234. *Mol. Plant Microbe Interact.* **16**, 743–751 (2003).
28. W. J. Dai, Y. Zeng, Z. P. Xie, C. Staehelin, Symbiosis-promoting and deleterious effects of NopT, a novel type 3 effector of *Rhizobium* sp. strain NGR234. *J. Bacteriol.* **190**, 5101–5110 (2008).
29. I. Sorg, U. M. Goehring, K. Aktories, G. Schmidt, Recombinant *Yersinia* YopT leads to uncoupling of RhoA-effector interaction. *Infect. Immun.* **69**, 7535–7543 (2001).
30. T. Coba de la Peña, E. Fedorova, J. J. Pueyo, M. M. Lucas, The symbiosome: Legume and rhizobia co-evolution toward a nitrogen-fixing organelle? *Front. Plant Sci.* **8**, 2229 (2018).
31. R. Atta *et al*., Pluripotency of *Arabidopsis* xylem pericycle underlies shoot regeneration from root and hypocotyl explants grown *in vitro*. *Plant J.* **57**, 626–644 (2009).
32. S. Boivin, C. Fonouni-Farde, F. Frugier, How auxin and cytokinin phytohormones modulate root microbe interactions. *Front. Plant Sci.* **7**, 1240 (2016).
33. T. Soyano, M. Hayashi, Transcriptional networks leading to symbiotic nodule organogenesis. *Curr. Opin. Plant Biol.* **20**, 146–154 (2014).
34. T. Soyano, H. Kouchi, A. Hirota, M. Hayashi, Nodule inception directly targets NF-Y subunit genes to regulate essential processes of root nodule development in *Lotus japonicus*. *PLoS Genet.* **9**, e1003352 (2013).
35. G. Nissan *et al*., The type III effectors HsvG and HsvB of gall-forming *Pantoea agglomerans* determine host specificity and function as transcriptional activators. *Mol. Microbiol.* **61**, 1118–1131 (2006).
36. D. R. Hann *et al*., The *Pseudomonas* type III effector HopQ1 activates cytokinin signaling and interferes with plant innate immunity. *New Phytol.* **201**, 585–598 (2014).
37. J. M. Vincent, *A Manual for the Practical Study of Root-Nodule Bacteria* (Blackwell Scientific Publications, Oxford-Edinburgh, UK, 1970), p. 164.
38. J. Sambrook, E. F. Fritsch, T. A. Maniatis, *Molecular Cloning: A Laboratory Manual* (Cold Spring Harbor Laboratory Press, Cold Spring Harbor, NY, ed. 2, 1989), p. 1659.
39. K. Bonaldi *et al*., The Nod factor-independent symbiotic signaling pathway: Development of *Agrobacterium rhizogenes*-mediated transformation for the legume *Aeschynomene indica*. *Mol. Plant Microbe Interact.* **23**, 1537–1544 (2010).
40. J. F. Mac Faddin, *Media for Isolation-Cultivation-Identification-Maintenance of Medical Bacteria* (Williams and Wilkins, Baltimore, MD, 1985), **vol. 1**, p. 966.
41. J. W. Tsai, M. R. Alley, Proteolysis of the McpA chemoreceptor does not require the *Caulobacter* major chemotaxis operon. *J. Bacteriol.* **182**, 504–507 (2000).
42. E. Giraud, J. Lavergne, A. Verméglio, Characterization of bacteriophytochromes from photosynthetic bacteria: Histidine kinase signaling triggered by light and redox sensing. *Methods Enzymol.* **471**, 135–159 (2010).
43. J. Wongdee *et al*., *nifDK* clusters located on the chromosome and megaplasmid of *Bradyrhizobium* sp. strain DOA9 contribute differently to nitrogenase activity during symbiosis and free-living growth. *Mol. Plant Microbe Interact.* **29**, 767–773 (2016).
44. K. Bonaldi *et al*., Large-scale transposon mutagenesis of photosynthetic *Bradyrhizobium* sp. strain ORS278 reveals new genetic loci putatively important for nod-independent symbiosis with *Aeschynomene indica*. *Mol. Plant Microbe Interact.* **23**, 760–770 (2010).
45. A. Renier *et al*., Photosynthetic *Bradyrhizobium* sp. strain ORS285 synthesizes 2-*O*-methylfucosylated lipochitooligosaccharides for *nod* gene-dependent interaction with *Aeschynomene* plants. *Mol. Plant Microbe Interact.* **24**, 1440–1447 (2011).
46. L. Marty *et al*., Structural basis for high specificity of amadori compound and mannopine opine binding in bacterial pathogens. *J. Biol. Chem.* **291**, 22638–22649 (2016).
47. N. Flaugnatti, L. Journet, Identification of effectors: Precipitation of supernatant material. *Methods Mol. Biol.* **1615**, 459–464 (2017).
48. D. Mattanovich *et al*., Efficient transformation of *Agrobacterium* spp. by electroporation. *Nucleic Acids Res.* **17**, 6747 (1989).